Three points bending ultrasonic fatigue resistance and vickers hardness of Tlalpujahua clay thermally treated

H.M. Venegas Montaño, V. López Garza, Luis Miguel Torres Duarte
Faculty of Mechanical Engineering, Universidad Michoacana de San Nicolás de Hidalgo (UMSNH), Santiago Tapia No. 403, Col. Centro, 5800, Morelia, Michoacán. México
0468633k@umich.mx, victor.garza@umich.mx, lmtorres@umich.mx

P. Martínez-Torres
Institute of Physics and Mathematics, Universidad Michoacana de San Nicolás de Hidalgo (UMSNH), Santiago Tapia No. 403, Col. Centro, 5800, Morelia, Michoacán. México
pablo.martinez@umich.mx

Gonzalo Mariano Domínguez Almaraz
Independent Researcher
dalmaraz@umich.mx

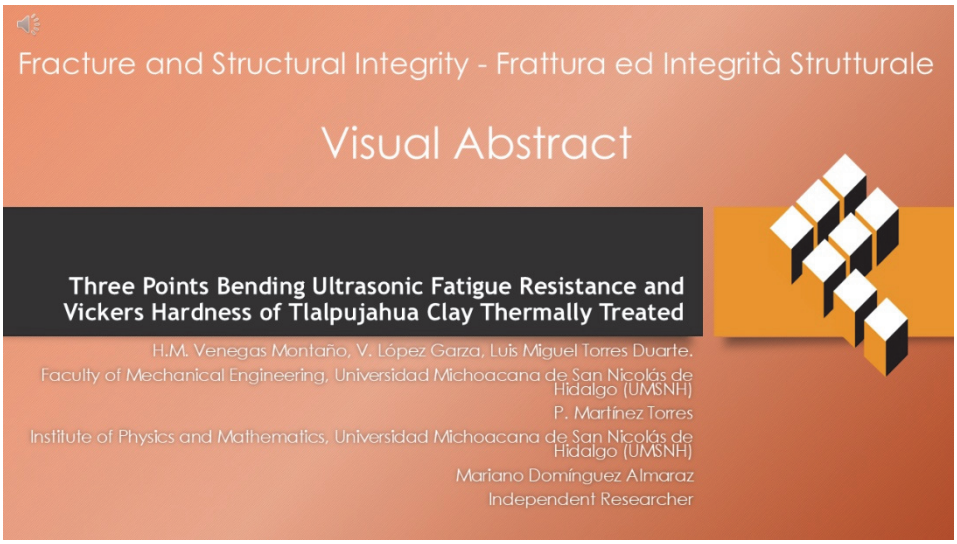

Citation: Venegas Montaño, H.M., Martínez-Torres, P., Garza, V. L., Torres Duarte, L. M., Three points bending ultrasonic fatigue resistance and vickers hardness of Tlalpujahua clay thermally treated, Fracture and Structural Integrity, 75 (2026) 157-166.

Received: 13.06.2025
Accepted: 18.10.2025
Published: 22.10.2025
Issue: 01.2026

KEYWORDS. Ultrasonic Fatigue, Clay, Mechanical Properties.

INTRODUCTION

The growing interest in predicting the lifetime of various materials, including ceramics, under very high fatigue cycles has contributed to the continuous advancement of the ultrasonic fatigue testing technique. This method applies cyclic loads to specimens, inducing resonance vibrations at ultrasonic frequencies. The test provides the material fatigue lifetime data with a certain number of cycles before failure, and it is possible to observe the crack propagation [1].
Clay ceramics have gained attention and continue to be studied for their chemical and physical properties due to their versatility and broad range of applications, from traditional uses in artistic crafts and kitchenware to their emerging role as a sustainable material [2]. Recent research in engineering highlights clay potential subjected to thermal treatments for use in structural applications and its combination with construction materials to enhance the thermal storage capacity of structural elements [3][4], as well as for improving its properties when combined with other materials as a phase change material [5].
The mechanical and physical properties of clay ceramics, such as hardness, porosity, and density, can significantly change under thermal treatment conditions, making it an attractive candidate for structural applications. Tlalpujahua clay, sourced from Michoacan, Mexico, contains a composition of silicon (Si), magnesium (Mg), calcium (Ca), potassium (K), aluminum (Al), iron (Fe), and sodium (Na), among others. The ability to harden after thermal treatment [6] enhances its mechanical performance, making it suitable for construction and industrial purposes [7].
Comprehensive characterization of clay's thermal and mechanical properties is fundamental for advancing the engineering applications of this material and exploring its potential for composite development. Recent studies have demonstrated the effectiveness of clay-based composites, such as clay soils reinforced with carbon fiber, in enhancing mechanical performance [8]. Furthermore, extensive research has been conducted on the behavior of clay under various loading conditions, including dynamic loading scenarios. For instance, Yi-Qun Tang et al. investigated the response of saturated soft clay surrounding tunnel structures subjected to vibration loads from Shanghai subway operations [9]; Géssica Soares Pereira et al. examined the effects of artificial cementation on tropical clay soils through ultrasonic analysis [10]. Given the diverse loading conditions encountered in practical applications, systematic investigation of clay's physicochemical composition and its correlation with mechanical properties under different loading regimes remains critical for material optimization and engineering design.
This work uses two techniques to study the mechanical properties of thermally treated clay bricks at different temperatures with a fixed holding time. The first technique involves ultrasonic fatigue, which is conducted under three bending conditions to determine the number of cycles until the clay brick fails, comparing the obtained results across different temperatures. The second technique utilizes Vickers indentation to measure changes in clay hardness relative to the treatment temperature. The effects of thermal treatment on physical properties, such as effective porosity and apparent density, were evaluated and used in an element finite model. This model aimed to calculate a von Mises equivalent stress under applied forces (ranging from 1 to 15 N) at the brick center. X-ray diffraction analysis was performed to identify chemical compounds present in the clay and their correlation with changes in hardness and fatigue life. The novelty of this study was taken from the fact that clay is a material composed of various compounds, which can result in diverse mechanical behaviors. In this context, mechanical tests were conducted on clays subjected to different heat treatments, providing novel insights into how temperature and mineralogical characteristics influence both hardness and fatigue behavior. Through a comparative analysis of Vickers hardness and ultrasonic fatigue, this work also provides initial guidance for designing clay-based structures under practical loading conditions.

EXPERIMENTAL PROCEDURES

Effective porosity and bulk density

Clay powder is mixed with water to create a mud consistency, which is then shaped into 36 small bricks, each with dimensions of 15 x 10 x 115 mm³ (see Fig. 1). After molding, the Tlalpujahua bricks are carefully dried at room temperature. The samples are then divided into three groups, each containing 12 bricks. These groups are subjected to thermal treatment in a Terlab Muffle with a controlled heating rate of 5 °C/min. Once the temperature is reached, the sample remains inside for 5 hours at temperatures of 500 °C (B1), 750 °C (B2), and 1000 °C (B3). After completing the time permanency, the samples were allowed to cool down to room temperature with the door closed to minimize thermal shock. Following the guidelines set by the International Society for Rock Mechanics (ISRM) [11], the effective porosity and bulk density of the thermally treated samples were determined using the equations [12]:

$$\varepsilon = \frac{V_{pore}}{V_{Bulk}} = \frac{\left(M_{SD} - M_D\right) / \rho_{water}}{\left(M_{SD} - M_S\right) / \rho_{water}} = \frac{M_{SD} - M_D}{M_{SD} - M_S} \tag{1}$$

$$\rho_{Bulk} = \frac{M_D}{M_{SD} - M_S} \rho_{water} \tag{2}$$

were ε and ρ_{Bulk} represent the effective porosity and bulk density, respectively; V_{pore} denotes the pore volume, V_{Bulk} indicates the bulk volume, M_D signifies the weight of the sample after undergoing the thermally treated and natural cooling process, M_S represents the saturated submerged weight of the sample, obtained by measuring the weight after immersing the sample in a distilled water for 48 h, M_{SD} refers to the saturated surface dry weight measured after 48 h when the sample is outside the water and dry with a cloth moist, and ρ_{water} denotes the density of the distilled water.

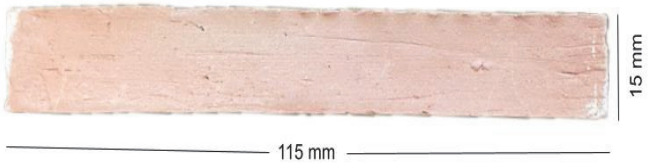

Figure 1: Typical clay bricks made for ultrasonic fatigue tests at 1000 °C.

The weight of each sample at various temperatures is measured using an analytical balance (ADAM equipment, ANimbus NBL-2141). The effective porosity and bulk density results are as follows: B1 samples exhibit an effective porosity of (32.4 ± 0.04) % and a bulk density of (1840 ± 4) kg/m³; B2 samples show an effective porosity of (32.9 ± 0.4) % and a bulk density of (1780 ± 5) kg/m³, and B3 samples have an effective porosity of (24.7 ± 0.2) % and a bulk density of (2030 ± 12) kg/m³. The slight increase in porosity observed between samples B1 and B2 can be attributed to the loss of carbonaceous matter through combustion and the development of thermal cracks, which occur within the temperature range of 500 °C to 700 °C during the dihydroxylation phase [13]. In contrast, sample B3 exhibits a substantial decrease in effective porosity, primarily due to shrinkage, as explained in [14]. Furthermore, some researchers suggest that this phenomenon may also be related to a secondary recrystallization process within the material [15].

Ultrasonic fatigue test

A custom-designed device fabricated with a 3D printer using PETG material with 100 % infill was developed for the ultrasonic fatigue tests. The device was specifically designed to secure and affix the testing brick, as depicted in Fig. 2a. This device enables the vertical translation of the brick through the use of two screws, as illustrated in Fig. 2b. The mechanism was developed to adjust the initial pressure, either increasing or decreasing it, once the device is positioned beneath the aluminum awl. Furthermore, a pressure sensor (Fig. 2c) has been integrated to determine precisely the force exerted by the custom-designed aluminum awl [16] at the midpoint of the brick.

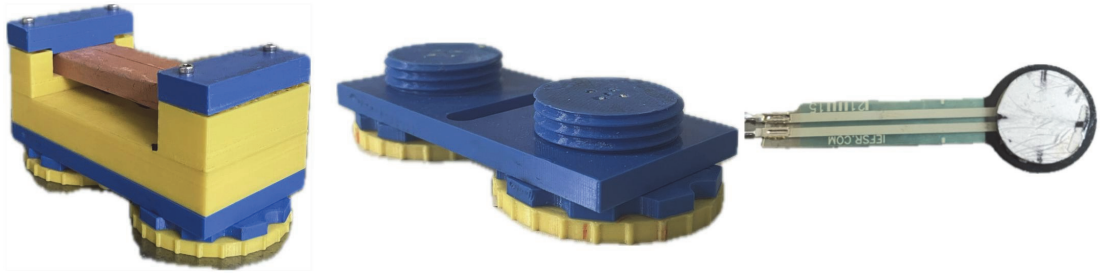

a) b) c)

Figure 2: (a) A self-designed device, (b) Screws for the vertical translation, (c) Pressure sensor.

An AISI 7075 aluminum awl (Fig. 3C) is utilized to apply a vibrating load of 20 kHz (modulated external driving force) onto the clay brick, as depicted in Fig. 3b. Before initiating the ultrasonic fatigue test, a fixed force was applied to the sample

brick to ensure consistent contact between the awl and the sample. The specific applied forces used for each sample are listed in Tab. 1. The amplitude vibration of the awl was 7 μm for all the experiments. Once the sample is mounted on the machine, the vibration starts and stops until the sample is fractured. This procedure was repeated for each set of samples, and the average number of cycles for the three temperatures of thermally treated samples was 810309 ± (3 %), 5056500 ± (17 %), and 2602609 ± (15 %) for B1, B2, and B3, respectively. These variations in cycle number are attributed to the thermal treatment, which affects each sample's hardness because the clay is undergoing crystal phase change transformations and grain growth.

Fig. 4 illustrates the temperature distribution of the brick captured by a thermographic camera within the first fifteen seconds of the ultrasonic test. These images reveal an increase in temperature at the center of the brick from 25 ºC (ambient temperature) to 42.9 °C during the first seconds of starting the experiment. Afterward, the temperature at that zone decreases to approximately 35 ºC during the fifteen seconds due to thermal energy dissipation.

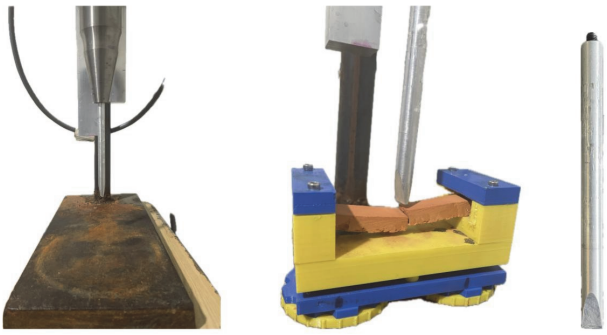

a) b) c)

Figure 3: (a) Ultrasonic fatigue machine, (b) Configuration to perform the ultrasonic fatigue over the clay brick, (c) Aluminum awl tip shape.

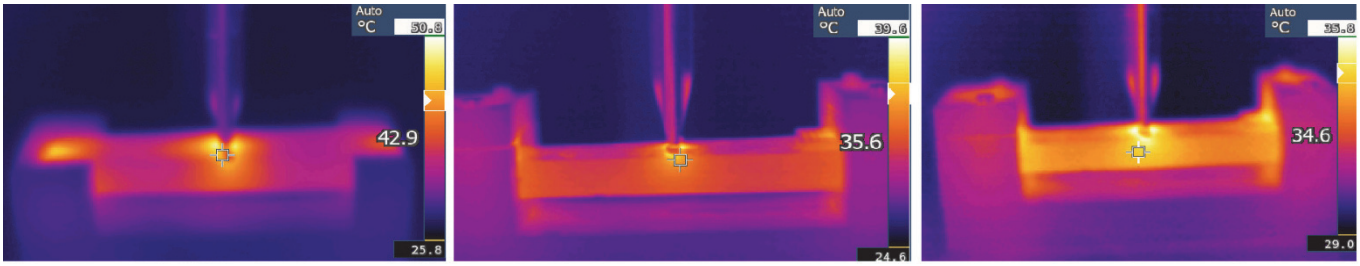

a) b) c)

Figure 4: Temperature of the sample, a) After 5 seconds of ultrasonic test, b) After 10 seconds of ultrasonic test, c) After 15 seconds of thermal equilibrium.

a) b) c)

Figure 5: Cross-sections of the fractured samples, thermally treated at (a) 500 °C, (b) 750 °C, and (c) 1000 °C.

Fig. 5 shows the images of the transversal section of bricks after fracturing for the three thermal treatments. There is a perceptible physical and optical difference between them. By visual inspection, the roughness decreases as the temperature of the thermal treatment increases. The RGB color code was identified using images of the thermal treatment clays (see Fig. 5), and their values were (135, 96, 60), (135, 92, 52), and (160, 112, 66) for the samples B1, B2, and B3, respectively. Sample B1, with thermal treatment at 500 °C, has a medium brown color; when the thermal treatment increases to 750 °C (sample

B2), it has a dark brown color, and sample B3, at 1000 °C, is light brown with orange tones. These color changes indicate the crystalline phase transformations the clay undergoes due to the thermal treatment. Furthermore, visual inspection reveals differences in the fractured characteristics of the samples as a function of temperature. A rough fracture surface is observed in the sample treated at 500 °C (B1), which is attributed to a combination of effective porosity and the material's hardness at this temperature. In contrast, samples B2 and B3 exhibit smoother fracture surfaces, which can be related to their increased sintering and the corresponding increase in hardness.

Vickers hardness and nanomechanical test instrument

Vickers indentation was performed using a Nanovea series Vickers indenter (Fig. 6a) with a 5 kg (49.0 N) load and a dwell time of 15 seconds to investigate the micro-hardness of the clay samples. A total of 15 cube-shaped samples, 10 x 10 x 10 mm^3 (Fig. 6b), were subjected to this procedure, with five samples tested for each temperature. Each sample underwent five indentations positioned at the corners and center of one face. The operational principle of the Vickers hardness testing system relies on the quantitative analysis of pyramidal indentation marks generated under controlled loading conditions, as depicted in Fig. 6c. The measurement protocol involves precisely determining the diagonal lengths of the square-shaped impression created by the diamond pyramid indenter, following the ASTM E384-17 standard specifications. Optical images were obtained using a Zeiss Axio Observer microscope. The Vickers hardness number is computed using the established relationship [17]:

$$HV = \frac{1.8544\,F}{d^2} \tag{3}$$

where HV represents the Vickers hardness number, F denotes the applied load in Newtons, and d corresponds to the arithmetic mean of the two diagonal measurements of the indentation, calculated as $d = \frac{d_1 + d_2}{2}$.

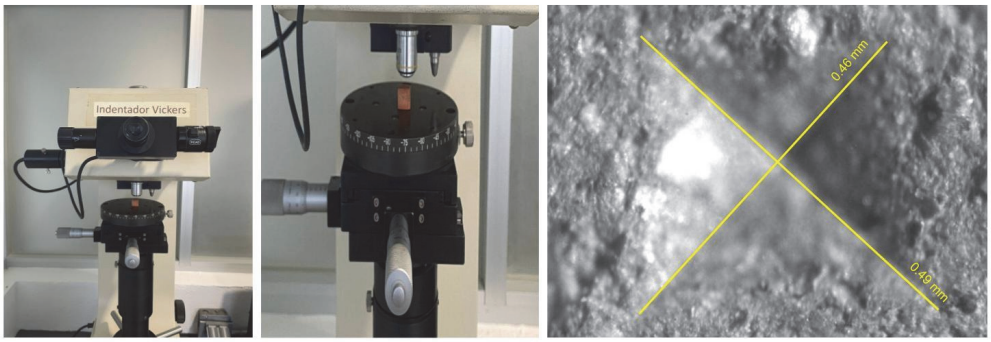

a) b) c)

Figure 6: a) Vickers indenter, b) A view of the cubic clay sample, c) Pyramid mark.

After analyzing the indentation images, where it was not observed any crack at the corners of the pyramid mark, the obtained Vickers hardness number for each temperature is as follows: B1 = 79.1 ± 2.7 HV (775.5 ± 26.8 MPa), B2 = 274.1 ± 14.6 HV (2688.0 ± 143.2 MPa), and B3 = 1057.8 ± 182.3 HV (10370.0 ± 1787.1 MPa). The results agree with what was reported by [18] in a study of kaolinite and illite under thermal treatment. The behavior of the obtained values shows an apparent increase in Vickers hardness with the increase in the thermal treatment temperature. This behavior can be partially attributed to the reduction in effective porosity; however, the significant increase in hardness in sample B3 is primarily a result of the chemical compound transformation, leading to permanent changes in hardening.

The crystalline chemical compounds were identified using X-ray diffraction (XRD) with a Siemens D5000 diffractometer equipped with Bragg-Brentano geometry and Cu-Kα radiation (λ=1.5418Å). Fig. 7 presents the XRD patterns of the samples: NTT (non-thermal treatment), B1, B2, and B3, highlighting the peaks corresponding to the compounds, such as quartz, illite, and their transformation into spinel at 1000 °C [19], gupetite, annite, pyroxene ideal, and hematite proto. The corresponding wt% and the formula of each compound are shown in Tab. 1.

Finite element software was used to simulate the von Mises stress behavior of a clay brick (15 × 115 × 10 mm^3) under varying physical property values, depending on the thermal treatment. The software required input data, including the bulk density obtained experimentally, as well as Young's modulus and Poisson's ratio, which were selected based on the literature.

According to the literature, Young's modulus exhibits a trend of increasing as a function of thermal treatment. However, during the dihydroxylation stage (300 °C to 800 °C), Young's modulus stabilizes or shows minimal growth until it experiences an exponential increase at temperatures exceeding 800 °C [20, 21]. Conversely, the Poisson's ratio demonstrated an inverse relationship with the Young's modulus: as the Young's modulus increased, the Poisson's ratio tended to decrease, and vice versa [22]. Considering this behavior, Young´s modulus of 1.2, 1.25, and 2.5 GPa and Poisson ratios of 0.31, 0.25, and 0.19 were chosen for B1, B2, and B3, respectively.

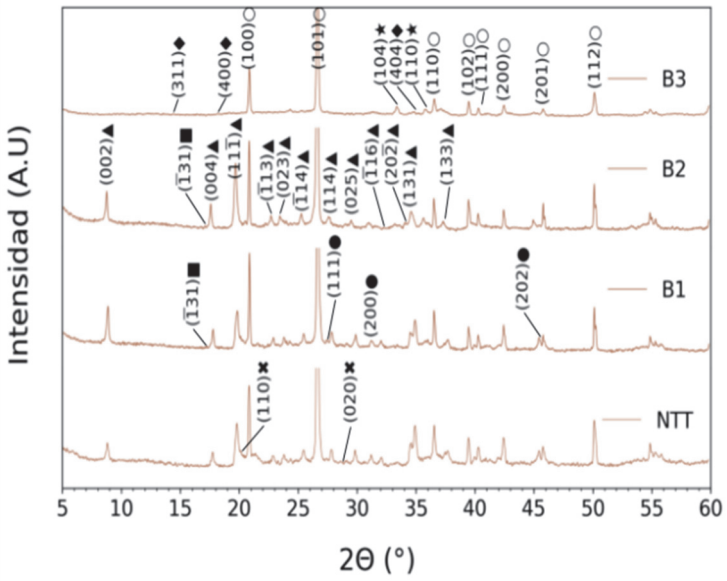

Figure 7: XRD patterns of Tlalpujahua clay thermally treated at different temperatures. The compounds are labeled as quartz, O; illite, ▲; gupeitite; annite,■; pyroxene-ideal, X; hematite proto, ★; and spinel, ◆.

Crystalline phases Formula (JCPDS) Samples	Quartz % (SiO2) 96-901-2601	Illite % (AlK2O12Si2) 96-900-9666	Guppetite % (Fe3Si) 96-901-4752	Annite % (Al2.52Fe2.312K0.92O12Si2.28) 96-900-2316	Pyroxene ideal % (MgO3Si) 96-900-2909	Hematite proto % (Fe1.76H0.06O3) 96-900-2162	Spinel % (Al2MgO2) 96-901-0352
NTT	61.1	36.7	1		1.2		
B1	62.4	34.6	0.6	2.4			
B2	71.1	26.0		2.9			
B3	89.8					7.6	2.6

Table 1: The phases detected in each sample match the reference patterns reported by the Joint Committee on Powder Diffraction Standards (JCPDS), with the corresponding JCPDS card numbers provided beneath each sample name [6].

The geometry of the underface of the aluminum awl tip (4 x 15 mm) was added as an additional element at the center of the simulated brick, where the applied force is between 1 and 15 N. (see Fig. 8a). Quadratic and tetrahedral meshes were considered in the finite element analysis. Fig. 8b illustrates the von Mises stress as a function of mesh density for both geometrical meshes. Based on the convergence study reported by [23], the quadratic mesh is shown to be the best option, as it not only converges from the beginning but also achieves a relative percentage error of 4% when using a mesh size of 0.004m. This result is consistent with the direction that higher mesh density yields a better solution. In contrast, the tetrahedral mesh exhibits a relative average percentage error of 27 % and does not show convergence in the von Mises results. The selected option was the quadratic mesh, with a size of 0.004 m, comprising 2907 nodes and 460 elements. The 3D CAD model of the brick with these mesh parameters is shown in Fig. 8c. The results of the mechanical simulations, using the information discussed above, are represented in Fig. 8d, where the behavior of the equivalent stress of each sample and the corresponding applied force is shown. The equivalent stress of each sample appeared to increase with the applied force. Furthermore, distinct variations were observed among the samples, where it was possible to discern that sample B1 exhibited the most significant deformation, while sample B3 displayed the slightest deformation.

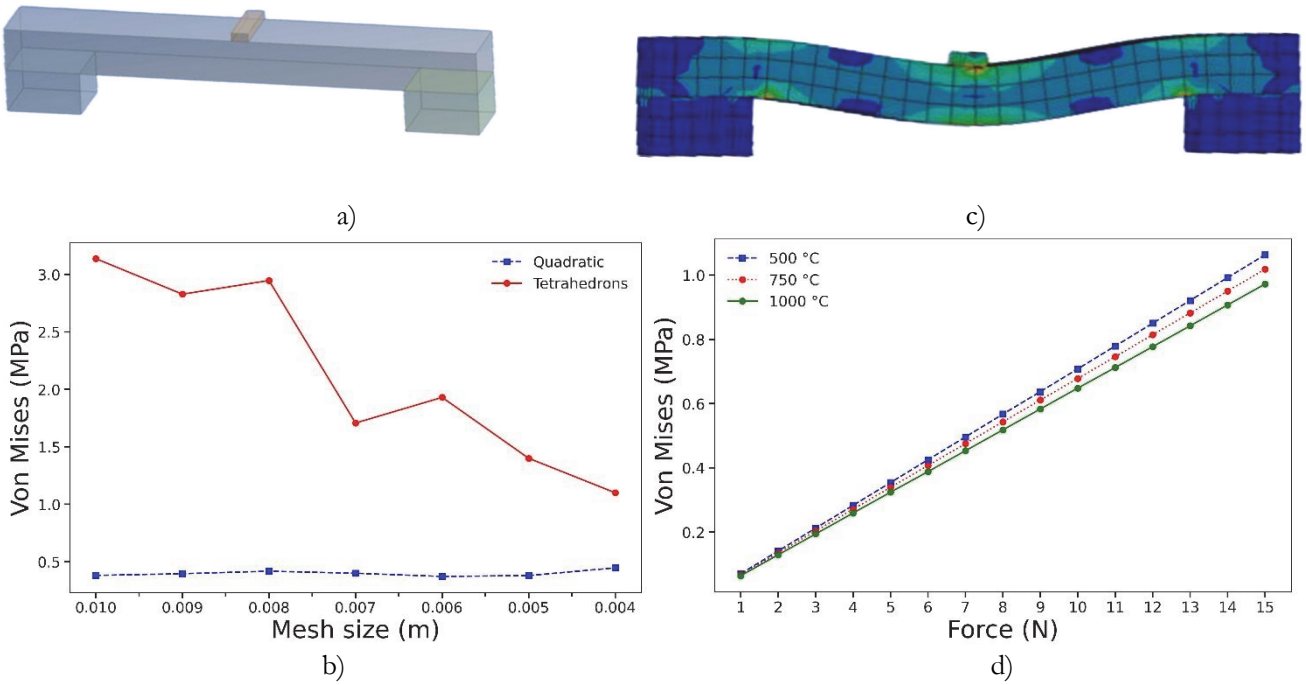

Figure 8: a) Simulation of the brick with the representation of the awl, (b) Mesh convergence analysis, c) Simulation of the brick and structure of the mesh, (d) Deformation von Mises as a function of the force applied for the samples B1, B2, and B3.

Discussion

The results obtained from the ultrasonic fatigue tests (lifetime in terms of number of cycles), Vickers hardness measurements, and finite element simulations show the mechanical behavior of thermally treated clay bricks (Tab. 2).

The ultrasonic fatigue analysis reveals a corresponding number of cycles for the thermal treatment temperature. The B1 samples (500 °C) exhibited the lowest fatigue resistance. This behavior can be attributed to the combined effects of effective porosity and low hardness. In contrast, the B2 sample (750 °C) exhibited high fatigue resistance, attributed to an increase in hardness while maintaining nearly the same effective porosity. However, sample B3 exhibited a shorter fatigue life than sample B2, partially due to illite transformation into spinel, a process known to generate microcracks within the microstructure [24]. These microcracks act as stress concentrators, promoting the initiation and propagation of cracks under cyclic and ultrasonic loading, which leads to reduced fatigue resistance.

The Vickers hardness results confirmed that increasing the thermal treatment temperature increases hardness, with B3 samples displaying the highest values. The reduction in effective porosity can partially explain this behavior. However, sample B2 exhibited an effective porosity value similar to B1; therefore, its higher hardness could be associated with the increment proportion of quartz and the simultaneous decrease in illite, a mineral known for its fragile nature (see Tab. 1). In the case of sample B3, the hardness increase can be attributed to a dual effect: the reduction in porosity and the crystalline transformations occurring at 1000 °C, particularly the disappearance of illite and its transformation into spinel, which, according to the literature, has a hardness between 2.89 GPa and 7.79 GPa [25].

The morphology of Tlalpujahua clay was analyzed using Scanning Electron Microscopy (SEM, JEOL JSM-7600F) operated at 15 kV and equipped with an Energy-Dispersive X-ray Spectrometer (EDS). The images reveal evidence of material densification. Figs. 9a and 9b display a similar morphology; however, in Fig. 9c, the smaller particles are almost absent, resulting in a more uniform surface and a denser structure. These observations are consistent with the increase in Vickers hardness observed at different thermal treatment temperatures.

Regarding the finite element simulation for obtaining von Mises strain, this study employs it to analyze the behavior of thermally treated clays under different loads. The results show a correlation with Vickers hardness, as both hardness and von Mises strain increase due to the thermal treatment temperatures. This behavior suggests that the mechanical properties of clays are significantly influenced by the temperature at which they are treated. However, this correlation is not observed

in the case of ultrasonic fatigue, indicating that to fully understand the behavior of thermally treated clays under ultrasonic fatigue conditions, it is essential to analyze the chemical composition changes induced by thermal treatment, such as the transformation of illite.

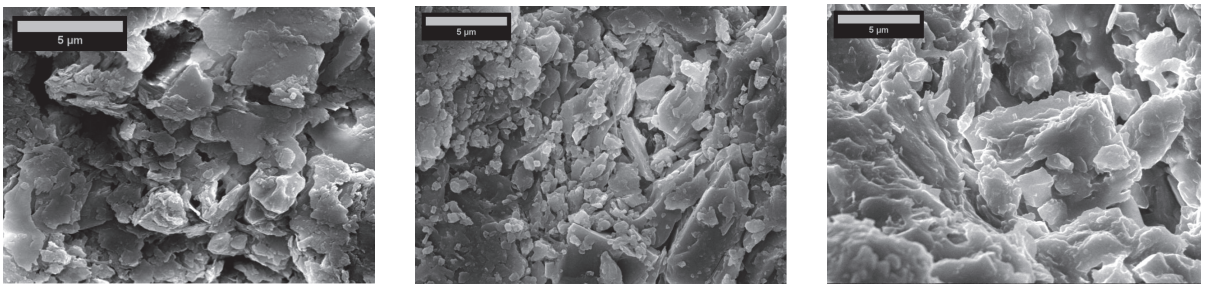

a) b) c)

Figure 9: SEM images of the firing treatment samples for Tlalpujahua at (a) 500 ◦C, (b) 750 ◦C, (c) 1000 ◦C.

The relationship between von Mises stress, ultrasonic fatigue, and hardness suggests that thermal treatment enhances mechanical strength but induces embrittlement, thereby increasing the material's susceptibility to fatigue failure. Although thermal treatment improves hardness and structural integrity, it simultaneously introduces brittleness at high temperatures, which may restrict its application in structural components exposed to ultrasonic fatigue conditions.

Sample	Force N	von Mises MPa	Hardness MPa	No. Cycles
B1	6.75	0.478	775 ± 3%	810309 ± 3%
B2	8.85	0.6	2688 ± 5%	5056500 ± 17%
B3	10.95	0.709	10370 ± 17%	2602609 ± 15%

Table 2: Results of von Mises deformation (simulation), Vickers Hardness, and Ultrasonic Fatigue.

CONCLUSIONS

- Ultrasonic fatigue tests were performed under a three-point bending loading modality with the brick samples thermally treated at different temperatures. The sample subjected to 750 °C demonstrated higher fatigue life due to a combination of effective porosity and hardness values.
- Heat treatment improves the mechanical properties of the clay but also induces embrittlement, which depends on the formation of microcracks due to mineralogical changes that occur at 1000 °C, restricting applicability in components under ultrasonic fatigue conditions.
- Tlalpujahua clay from Mexico was analyzed and subjected to thermal treatments at 500°C (B1), 750°C (B2), and 1000°C (B3). Mechanical and physical properties, including effective porosity, bulk density, and Vickers hardness, were determined for each temperature. These changes were characterized using various experimental techniques and validated through simulations. The simulation results were in agreement with the experimental findings of Vickers hardness.
- X-ray diffraction analysis revealed that at 1000 °C, illite transformed into spinel, contributing to a dramatic increase in hardness and a decrease in effective porosity. These changes contributed to the increase in Young's modulus and Vickers hardness of the clay from 79 HV at 500 °C to 1058 HV at 1000 °C.
- Further research is required to fully understand the behavior of clay, as heat treatment can induce microcrack formation, grain growth, densification, and sintering kinetics, all of which strongly affect its mechanical properties. Although this study provides an advance in the understanding of clay's mechanical behavior, further experimentation with different methods is necessary to expand the characterization. Complementary tests, such as fracture toughness and flexural strength, would provide valuable insights into the material's response to applied loads and clarify the role of microstructural defects in overall performance.

ACKNOWLEDGMENT

The authors acknowledge SECIHTI for financial support through projects: phD scholarship, postdoctoral fellowship. Also, partially funded by the project ICTI-Michoacán ICTI-PICIR23-009.

The analyses of XRD were carried out in the National Nano and Biomaterials Laboratory, Cinestav-IPN; Funded by projects FOMIX-Yucatán 2008-108160, CONACYT LAB-2009-01-123913, 292692, 294643, 188345 and 204822. Thanks to Dr. Patricia Quintana for access to LANNBIO, M.C. Daniel Aguilar Treviño for obtaining the diffractograms and M.C. Mario Herrera Salvador for corrective maintenance of the D-8 Advance diffractometer.

The analyses of Vickers Hardness were carried out in the Instituto de investigación en Metalurgia y Materiales (IIMM) of the Universidad Michoacana de San Nicolás de Hidalgo. Thanks to M.C. Héctor Damian Orozco Hernández for the support provided for the Vickers hardness test. We want to express our gratitude to Mrs. Issi Lucía Murillo Balderas for her help in reviewing and correcting the English writing of this article. Their time, effort, and expertise were essential in improving the quality of the manuscript.

REFERENCES

[1] Mayer, H. (2016). Recent developments in ultrasonic fatigue. Fatigue & Fracture of Engineering Materials & Structures, 39(1), pp. 3-29.

[2] Muntari, M. Y. and Windapo, A. O. (2021, May). Clay as a Sustainable Building Material and Its Benefits for Protection in the Built Environment. In IOP Conference Series: Materials Science and Engineering, 1144(1), 012044).

[3] Memon, S. A. (2014). Phase change materials integrated in building walls: A state of the art review. Renewable and sustainable energy reviews, 31, 870-906.

[4] Lan, Y., Liu, Y., Li, J., Chen, D., He, G. and Parkin, I. P. (2021). Natural clay-based materials for energy storage and conversion applications. Advanced Science, 8(11), 2004036.

[5] Salgueiro, T., Samagaio, A., Gonçalves, M., Figueiredo, A., Labrincha, J. and Silva, L. (2021). Incorporation of phase change materials in an expanded clay containing mortar for indoor thermal regulation of buildings. Journal of Energy Storage, 36, 102385.

[6] Venegas, H. M., Almaraz, G. M. D., Gómez-Ortiz, N. M., Montes-de-Oca, L. M., Servín-Campuzano, H., González-Avilés, M., Martínez-Torres, P. (2025). The effect of mineral composition and porosity on the thermal conductivity of clay induced by firing processes at different temperatures and holding times. Materials Chemistry and Physics, 333, 130325.

[7] Hernández García, L. C., Monteiro, S. N. and Lopera, H. A. C. (2024). Recycling Clay Waste from Excavation, Demolition, and Construction: Trends and Challenges. Sustainability, 16(14), 6265.

[8] Bao, X., Huang, Y., Jin, Z., Xiao, X., Tang, W., Cui, H. and Chen, X. (2021). Experimental investigation on the mechanical properties of clay soil reinforced with carbon fiber. Construction and Building Materials, 280, 122517.

[9] Tang, Y. Q., Cui, Z. D., Zhang, X. and Zhao, S. K. (2008). Dynamic response and pore pressure model of the saturated soft clay around the tunnel under vibration loading of Shanghai subway. Engineering Geology, 98(3-4), pp. 126-132.

[10] Pereira, G. S., Pitanga, H. N., Ferraz, R. L., Rodrigues, R. A., da Silva, T. O. and Nalon, G. H. (2024). Ultrasonic analysis of artificial cementation effects on tropical clay soils. Geotechnical and Geological Engineering, 42(4), pp. 2529-2553.

[11] Jaber, H., Maalouf, E., Yehya, A., Salah, M.K., Bou-Hamdan, K., Harb, M. (2024). The effect of temperature on the mechanical and hydraulic properties of sedimentary rocks, Geoenergy Science and Engineering, 235, 212702. DOI: https://doi.org/10.1016/j.geoen.2024.212702.

[12] Lin, W., Tadai, O., Takahashi, M., Sato, D., Hirose, T., Tanikawa, W., Hamada, Y., Hatakeda, K. (2015). An Experimental Study on Measurement Methods of Bulk Density and Porosity of Rock Samples, Journal of Geoscience and Environment Protection, 03(05), pp. 72–79. DOI: https://doi.org/10.4236/gep.2015.35009.

[13] Trindade, M.J., Dias, M.I., Coroado, J., Rocha, F. (2009). Mineralogical transformations of calcareous rich clays with firing: A comparative study between calcite and dolomite rich clays from Algarve, Portugal, Appl Clay Sci, 42(3–4), pp. 345–355. DOI: https://doi.org/10.1016/j.clay.2008.02.008.

[14] Searle, A. B. (1924). The chemistry & physics of clays and other ceramic materials. E. Benn limited.

[15] Wong-Ng, W. (2019). Ceramic materials.Wiley.

[16] Almaraz, G.M.D., Sánchez, R.H., Martínez, A.G., Gómez, E.C., Juárez, J.C.V., Garza, V.L. (2017). Ultrasonic Fatigue Tests on the Nafion Proton Exchange Membrane, under the Modality of Three Points Bending., Procedia Structural Integrity, 3, pp. 571–578.

[17] Corredor, E., González-Estrada, O. A. and Ospina-Ospina, R. (2022). Deposición de láser pulsado de hidroxiapatita en Ti-6Al-4V producido por manufactura aditiva. Revista UIS Ingenierías, 21(4), pp. 107-121.
[18] Sidjanin, L., Rajnovic, D., Ranogajec, J., Molnar, E. (2007). Measurement of Vickers hardness on ceramic floor tiles, J Eur Ceram Soc, 27(2–3), pp. 1767–1773. DOI: https://doi.org/10.1016/j.jeurceramsoc.2006.04.150.
[19] Widjonarko, D.M., Wahyuningsih, S., Pramono, E., Saraswaty, T.E., Lestari, W.W., Rahardjo, S.B., April, S. (2022). Material characterization of pagerjurang clay as a raw material for pottery., Journal of Physics: Conference Series, 2190.
[20] Húlan, T., Trník, A., Štubňa, I., Bačík, P., Kaljuvee, T., Vozár, L. (2015). Development of young's modulus of illitic clay during heating up to 1100°C, Medziagotyra, 21(3), pp. 429–434. DOI: https://doi.org/10.5755/j01.ms.21.3.7152.
[21] Nigay, P.M., Cutard, T., Nzihou, A. (2017). The impact of heat treatment on the microstructure of a clay ceramic and its thermal and mechanical properties, Ceram Int, 43(2), pp. 1747–1754. DOI: https://doi.org/10.1016/j.ceramint.2016.10.084.
[22] Alzo'ubi, A.K., Alneasan, M. (2022). Experimental study on the effect of thermal treatment on the mechanical properties of clay-rich rocks (mudstone), Results in Engineering, 16. DOI: https://doi.org/10.1016/j.rineng.2022.100728.
[23] Okereke, M., Keates, S. (2018). Finite element mesh generation., Springer Tracts in Mechanical Engineering, Springer International Publishing, pp. 165–186.
[24] Sedmale, G., Sperberga, I., Sedmalis, U. and Valancius, Z. (2006). Formation of high-temperature crystalline phases in ceramic from illite clay and dolomite. Journal of the European Ceramic Society, 26(15), pp. 3351-3355.
[25] Bhaduri, S., & Bhaduri, S. B. (2002). Microstructural and mechanical properties of nanocrystalline spinel and related composites. Ceramics international, 28(2), 153-158.